Texturization and Light Trapping in Silicon Solar Cells


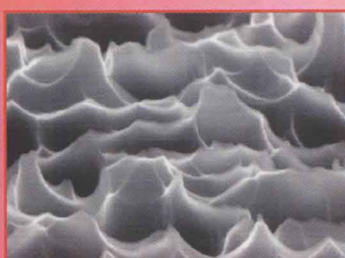


U. Gangopadhya
S. K. Dutta
H. Saha

Novinka

TEXTURIZATION AND LIGHT TRAPPING IN SILICON SOLAR CELLS

U. GANGOPADHYA,
S. K. DUTTA
AND
H. SAHA

Nova Science Publishers, Inc.
New York

LIBRARY OF CONGRESS CATALOGING-IN-PUBLICATION DATA

Gangopadhyay, U.
Texturization and light trapping in silicon solar cells / U. Gangopadhyay, S. K. Dutta and H. Saha, authors.
p. cm.
ISBN 978-1-60692-081-7 (softcover)
1. Silicon solar cells. 2. Photovoltaic power generation. I. Dutta, S. K. II. Saha, H. III. Title.
TK2960.G35 2009
621.31'244--dc22

2008041990

Published by Nova Science Publishers, Inc. New York

TEXTURIZATION AND LIGHT TRAPPING IN SILICON SOLAR CELLS

PREFACE

Reduction of optical losses in both mono and multicrystalline silicon solar cells by surface texturing is one of the important issues of modern silicon photovoltaics. Texturing of the front surface of silicon solar cells has been modeled and analyzed with reference to the reduction in reflection co-efficient and increase in optical trapping. Significant enhancement in open circuit voltage and short circuit current has been achieved through such texturing of the front surface of mono-silicon solar cells. A proper optimization of texture angle appears to be important for the best performance of the solar cells. An alternative way of reducing the surface reflection and enhancement of the cell parameters is to produce to passive front surface porous silicon layer. An analysis of the characteristics of a porous silicon layer shows that the morphology of the layer is an important design parameter.

To realize the structures in practice, several methods are available, but many of this method are either not cost effective or commercially non available. In order to achieve good uniformity of pyramidal textured structure of the silicon surface, a mixture of NaOH/KOH and isopropyl alcohol (IPA) is generally used for texturization of mono crystalline solar cells. However, due to high cost of IPA, there is always search for alternative source. This source should not only be cost effective but should also result in reduced interfacial energy between silicon and ionized electrolyte chemical solution to achieve sufficient wet-ability for the silicon surface in order to enhance pyramid nucleation. Different novel texturization techniques for monocrystalline silicon are descried in this chapter including solar cells performance.

For multicrystalline silicon (mc-Si) solar cells, the standard alkaline solution of NaOH/KOH does not produced textured surface of good quality so as to give satisfactory open circuit voltage and efficiency. This is because of grain boundary delineation with step formed between successive grains of different orientations. Different novel texturization techniques for multicrystalline silicon are also included in this chapter including solar cells performance.

CONTENTS

Chapter 1

INTRODUCTION

Texturing of the front and/or back surfaces of a solar cell surfaces to improve their performances has been attempted since the year 1960 [1]

The major objectives of texturing are [2, 3]

(i) reduction of front surface reflectance,
(ii) increase in the path length of the entered light of lower wavelengths by oblique trajectory within the cell and absorption of light closer to the junction,
(iii) optical trapping of weakly absorbed light by multiple internal reflections from the top and bottom surfaces of the cell thereby also increasing the optical path length. The increased path length with an oblique trajectory leads to an effective increase in the absorption co-efficient.

All these effects lead to the realization of higher performance thick cells and also efficient solar cells of comparatively lower thickness (thin cell), which significantly reduces the material cost without degrading the cell performance.

In this chapter, we will discuss the texturing in silicon solar cells pointing out its role in enhancement of the solar cell parameters like short circuit current, open circuit voltage and efficiency. We will also discuss recent research trends in experimentally obtaining the desired texture and the viability in the commercial / industrial use of these methodologies.

Section 2 summarizes the various models of texturization and presents simple model calculations to elaborate the role of texturization in enhancing the cell performance.

Section 3 discusses the various technologies in realizing texturization in mono-crystalline silicon solar cells along with their comparative analysis.

Section 4 deals with the results of the improvements in solar cell parameters that occur due to various texturization schemes and explores the cost effective efficient choice of suitable texturization.

Section 5 discusses the technology and its role on the efficiency of multi-crystalline silicon solar cell, along with their suitability for industrial applications.

Chapter 2

MODELS OF TEXTURIZATION

Various texturing geometries to reduce reflection co-efficient and to trap weakly absorbed light have been proposed and analyzed [1 – 12]

The different texturing schemes include :

1] Lambertian geometry,
2] Upright pyramid geometry,
3] Slat or Micro-grooved geometry,
4] Inverted Pyramid geometry,
5] Simple prism pyramid geometry,
6] Grating geometry,
7] Three Perpendicular planes (3PP) geometry,
8] Perpendicular slat geometry,
9] Porous silicon

We will first examine analytically the effect of texturization by considering a slat (micro-grooved V –shaped) texturing geometry. This is one of the common texturing geometries usually investigated for their role in the reduction of front surface reflectance and for their light trapping characteristics [13-17]. The results also closely resemble the analysis for upright rectangular regular pyramid texturing on the front surface. We will then consider different structures of texturization and make a comparative analysis between them.

2.1. SILICON SOLAR CELL WITH MICRO-GROOVED FRONT SURFACE AND LAMBERTIAN (RANDOMLY TEXTURED) BACK SURFACE

2.1.1. Reflection Coefficient of Micro-Grooved Silicon Front Surface

We consider a silicon solar cell for which the schematic diagram is shown in Figure 1. It assumes a slat type micro-grooved structure at the front surface [18].

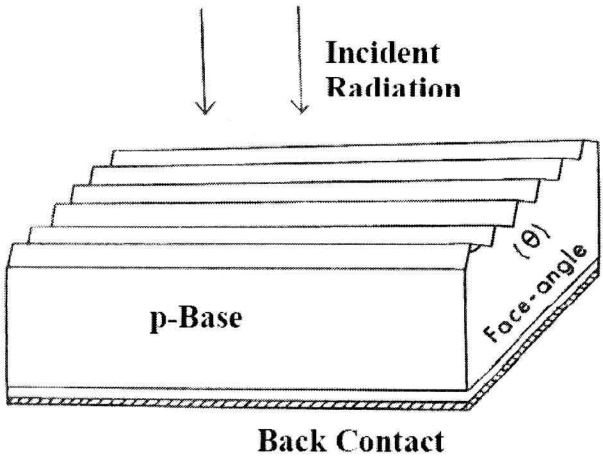

Figure1. Schematic diagram of a silicon solar cell.

For a given slat angle of silicon surface, the reflection coefficient at a particular wavelength decrease in comparison with the planar silicon surface due to multiple reflection at the front surface [7].

For a beam of light incident perpendicular to the base of the solar cell, the number of reflections before the light escapes from the front surface depends critically on the slat angle. When the slat angle θ satisfies the condition [13]

$$\theta = 180/m \tag{1}$$

or

$$\theta = 180/(m + 0.5) \tag{2}$$

where m=1,2,3,4,....., all rays escape after undergoing m reflections either vertically [when eq.(1) is satisfied] or parallel to the one of the refracting sides [when eq. (2) is satisfied] [7].

When the slat angle θ lies in the range,

$$180/(m+1)<\theta<180/(m+½),\ m=1,2,3,4, \tag{3}$$

a fraction of the incident rays undergo m+1 reflections while the rest have m reflections, the fraction being given by

$$f_m=\frac{\cos\phi_{m+1}}{\cos\phi_1}, \tag{4}$$

where Φ_{m+1} [=|90 – (m+½)θ|] is the (m+1)th incident angle and Φ_1(=90-½θ) the first incident angle.

Therefore, once a slat angle is specified, the number of reflections and the fraction of the incident rays undergoing it are obtained through the equations (1) - (4).

The total reflection coefficient $R_F(\lambda, \theta)$ of the silicon surface is a function of wavelength of incident light for a given slat angle and is obtained from Fresnel's equations [18] and is given by

$$R_F(\lambda,\theta)=R_m(\lambda,\theta),\text{when } 180/(m+1/2)<\theta<180/m \tag{5}$$

and

$$R_F(\lambda,\theta)=R_m(\lambda,\theta)+f_m[R_{m+1}(\lambda,\theta)-R_m(\lambda,\theta)]\text{, when } 180/(m+1)<\theta<180/(m+½) \tag{6}$$

where R_m is given by,

$$R_m(\lambda,\theta)=\frac{1}{2}\left(\prod_{i=1}^{m}R_p(i)+\prod_{i=1}^{m}R_N(i)\right), \tag{7}$$

where

$$R_p(i)\left(=\frac{\tan^2(\phi_i-\phi_i^{'})}{\tan^2(\phi_i+\phi_i^{'})}\right)$$

and

$$R_N(i)\left(=\frac{\sin^2(\phi_i-\phi_i^{'})}{\sin^2(\phi_i+\phi_i^{'})}\right)$$

$R_p(i)$ and R_n (i) are dependent on the wavelength of light through the dependence of ϕ_i, the ith incident angle and $\phi_i^{'}$, the ith refracted angle, on the refractive index.

Figure 2 shows the calculated values of reflection coefficient of textured silicon surface as a function of wavelength for different slat angles. The curve for which θ=180° corresponds to a planar silicon surface. It is observed that the calculated values agree extremely well with those reported for a planar surface as well as for a textured surface of 70.5° slat angle [18].

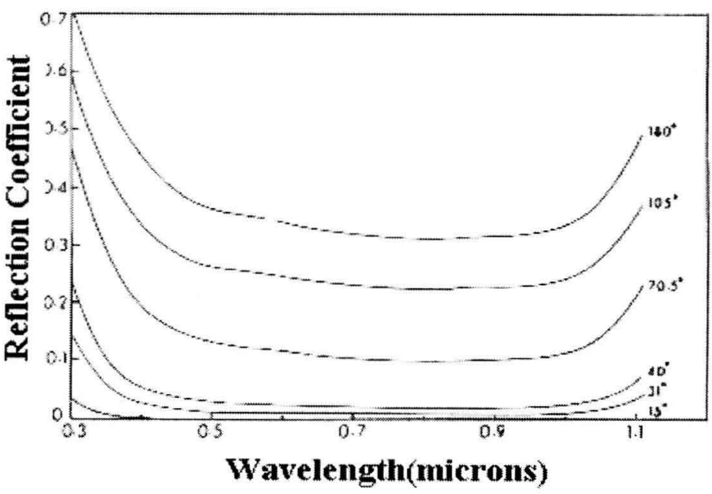

Figure 2. Reflection co-efficient of silicon with front surface slat texture as a function of wavelength for different slat angles.

It may be noted that the reflection coefficient values remain the same as that for a planar surface as long as the slat angle is larger than 120°. For the slat angles θ for which 120° <θ <180°, there can be only one reflection and the reflection coefficient, therefore, virtually remains the same. The reflection coefficient values for a given wavelength are found to decrease monotonically with the decrease in slat angle (for θ<120°) and for the slat angles less than 20°, the reflection coefficient reduces to almost zero. However, the reflection coefficient varies in a discontinuous fashion with the slat angle. This is related to the fact that number of reflections changes abruptly as the slat angle decreases. When the slat angle is decreased below 120^0, a fraction of the rays undergoes two reflections before escaping, while the incident rays near the top of the slats leave after only one reflection. At $\theta=90^0$, all the incident rays will have two reflections. For 90° <θ <72°, a fraction of the incident rays will leave after 3 bounces, while the rest will have only two reflections, For different ranges of slat angles of the micro-grooved solar cells, the number of reflections that the incident ray experiences before leaving is shown in the following table 1.

Table 1. Number of reflections from the micro-grooved surface with different slat angles

Slat angle (θ)	No. of reflection (m)	Direction of outgoing ray
180°	1	V
180°-120°	1	NVP
120°	1	P
120°-90°	1<m<2	NVP
90°	2	V
90°-72°	2<m<3	NVP
72°	2	P
72°-60°	2<m<3	NVP
60°	3	V
60°-51.43°	3<m<4	NVP
51.43°	3	P
51.43°-45°	3<m<4	NVP
45°	4	V
45°-40°	4<m<5	NVP
40°	4	P
40°-36°	4<m<5	NVP
36°	5	V
36°-32.72°	5<m<6	NVP

Table 1. Continued

Slat angle (θ)	No. of reflection (m)	Direction of outgoing ray
32.72°	5	P
32.72°-30°	5<m<6	NVP
30°	6	V
30°-27.69°	6<m<7	NVP
27.69°	6	P
27.69°-25.71°	6<m<7	NVP
25.71°	7	V
25.71°-24°	7<m<8	NVP
24°	7	P
24°-22.5°	7<m<8	NVP
22.5°	8	V
22.5°-21.18°	8<m<9	NVP
21.18°	8	P
21.18-20°	8<m<9	NVP
20°	9	V

P: Parallel to the groove V: Vertical to the base, NVP: Neither parallel nor vertical .

2.1.2. Reflection Coefficient of the Micro-Grooved Silicon Surface with AR Coating for Different Slat Angles

In this section, we examine whether an AR coating on a textured surface further reduces the reflection co-efficient [14]. A single layer AR coating is assumed to be present on the front micro-grooved surface shown in Figure 1 and Figure 3. We also study the role of flat regions [Fig 3] between the sloping faces of the textures, the width of which appears to be an important parameter in determining the overall reflection.

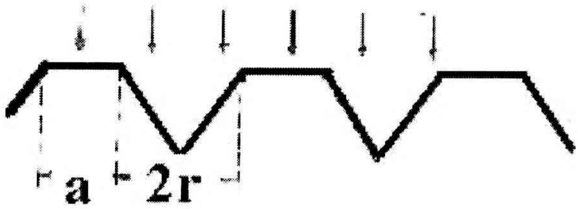

Figure 3. Schematic diagram of textured silicon front surface with flat regions.

For a beam of light incident normal to the base of solar cell, the number of reflections (m) that the light undergoes before escaping depends on the slat angle and can be calculated in accordance with the equations (1-4).

Reflection Coefficient for Micro-Grooved Silicon Surfaces without Flats

In the presence of an AR coating, the total reflection coefficient $R_G(\lambda,\theta)$ of the silicon surface as a function of the wavelength of the incident light for a given slat angle is obtained from Fresnel's equations and is given by [13]

$$R_G(\lambda,\theta)=R_m(\lambda,\theta), \tag{8}$$

when $[180/(m+1/2)]<\theta<(180/m)$ and

$$R_G(\lambda,\theta)=R_m(\lambda,\theta)+f_m\{R_{m+1}(\lambda,\theta)-R_m(\lambda,\theta)\}, \tag{9}$$

when $[180/(m+1)]<\theta<[180+m(m+1/2)]$, the fraction f_m being given by,

$$f_m=\frac{\cos\gamma_{m+1}}{\cos\gamma_1},$$

and R_m is given by,

$$R_m(\lambda,\theta)=(1/2)\left[\prod_{i=1}^{p}R_p(i)+\prod_{i=1}^{n}R_N(i)\right].$$

The expression for $R_p(i)$ and $R_N(i)$ which are, respectively, the parallel and normal reflection components for the i th reflection can be obtained following an analysis by Sopori and Pryor [18] and are expressed as

$$R_P(i)=\frac{\left[r_{ap}(i)+r_{sp}(i)\cos\delta_i\right]+r_{sp}(i)\sin^2\delta_i}{\left[1+r_{ap}(i)r_{sp}(i)\cos\delta_i\right]^2+\left[r_{ap}(i)r_{sp}(i)\sin\delta_i\right]^2},$$

$$R_N(i)=\frac{\left[r_{an}(i)+r_{sn}(i)\cos\delta_i\right]+r_{sn}(i)\sin^2\delta_i}{\left[1+r_{an}(i)r_{sn}(i)\cos\delta_i\right]^2+\left[r_{an}(i)r_{sn}(i)\sin\delta_i\right]^2}$$

where

$$r_{ap}=\frac{\tan\left(\gamma_i-\gamma_i^{'}\right)}{\tan\left(\gamma_i+\gamma_i^{'}\right)},r_{an}(i)=-\frac{\sin\left(\gamma_i-\gamma_i^{'}\right)}{\sin\left(\gamma_i+\gamma_i^{'}\right)},$$

and

$$r_{sp}=\frac{\tan\left(\phi_i-\phi_i^{'}\right)}{\tan\left(\phi_i+\phi_i^{'}\right)},r_{sn}(i)=\frac{\sin\left(\phi_i-\phi_i^{'}\right)}{\sin\left(\phi_i+\phi_i^{'}\right)}$$

are the Fresnel coefficients at the air-AR interface and AR-silicon interface, respectively. The expression for δ_i for the ith reflection is given by [18]: $\delta_i=(4\pi/\lambda)nt\cos\gamma_i, n$ being the refractive index of the AR coating material and t is the thickness of AR coating. The angles γ_i, $\gamma_i^{'}$, ϕ_i, $\phi_i^{'}$ refer to the angles of incidence and reflected rays at the air-AR interface and AR-silicon interface respectively for the ith reflection (Figure 4). It is clear from the Figure 4 that $\gamma_i^{'}=\phi_i$,

The ith incident angle at the air-AR coating interface is calculated from [13]

$$\gamma_i=\left|90^{\circ}-(i-1/2)\theta\right|.$$

Similarly,

$$\gamma_i^{'}=\phi_i=\sin^{-1}(\sin\gamma_i/n),$$

and

$$\phi_i^{'}=\sin^{-1}(\sin\gamma_i/\mu),$$

n_s being the refractive index of silicon.